Ceramics International 50 (2024) 37033–37040

Contents lists available at ScienceDirect

Ceramics International

journal homepage: www.elsevier.com/locate/ceramint

Tailoring the crystalline and amorphous phase ratios of TiO_2 through the use of organic additives during hydrothermal synthesis

Nejc Rozman [a,1], Andrijana Sever Škapin [a,b], David M. Tobaldi [c], Goran Dražić [d], Peter Nadrah [a,*]

[a] Slovenian National Building and Civil Engineering Institute, Dimičeva ulica 12, 1000, Ljubljana, Slovenia
[b] Faculty of Polymer Technology - FTPO, Ozare 19, 2380, Slovenj Gradec, Slovenia
[c] CNR NANOTEC, Institute of Nanotechnology, University Campus Ecotekne, Via per Monteroni, 73100, Lecce, Italy
[d] Department of Materials Chemistry, National Institute of Chemistry, Hajdrihova ulica 19, 1000, Ljubljana, Slovenia

ARTICLE INFO

Handling Editor: Dr P. Vincenzini

Keywords:
Sol-gel processes (A)
X-ray methods (B)
Chemical properties (C)
TiO_2 (D)
Photocatalysis

ABSTRACT

The photocatalytic properties of TiO_2 are primarily determined by its crystallinity and crystalline phase ratios. To improve the photocatalytic properties of TiO_2, greater control over the formation of crystalline and amorphous phases during synthesis is therefore required. In this study, we demonstrate how the addition of minute amounts of three organic compounds (isopropanol, acetone and acetic acid) during hydrothermal treatment affects the amorphous and crystalline phase ratios: the addition of isopropanol or acetone accelerates the phase transition from anatase and brookite to rutile, whereas the addition of acetic acid inhibits the transformation of anatase to rutile, increasing the content of amorphous phase compared to samples where no organic compound was added. We show that the combination of the organic compound added, along with the duration of the hydrothermal treatment, can be used to tailor the phase composition of TiO_2, so as to obtain either: i) TiO_2 with a high content of both rutile and amorphous phase, ii) TiO_2 with a high rutile content and iii) TiO_2 with different ratios of all four phases, when the duration of synthesis is short (2–4 h). The materials synthesized exhibited high photocatalytic activity (in most cases higher than P25), which is attributed to the beneficial phase composition and high specific surface area.

1. Introduction

TiO_2 is chemically stable and biologically inert, non-toxic and does not release chemicals into the environment, which can be a concern with some other photocatalysts [1]. These favourable properties make titanium dioxide one of the most promising photocatalysts for various applications. To fully utilize the potential of TiO_2, however, it is important to properly tailor its properties, including the amount and distribution of crystalline and amorphous phases, the ratio of crystalline phases, any exposed crystal facets, the band gap energy, particle size, and specific surface area [2–4]. These properties influence the photocatalytic properties of the material and can be tailored through modification of the synthesis procedure. TiO_2 can be doped and modified with other materials, so as to influence a crucial property of the photocatalyst, i.e. the ratio between the crystalline phases (anatase, brookite and rutile) and the amount of amorphous phase. It is therefore important to understand the influence of the synthesis parameters on the final phase ratios and thus be able to propose the optimal synthesis procedure for the phase ratios desired. These parameters depend on the synthesis procedure used and the crystallization step. It is well known that, in the absence of any other modification, the use of an annealing temperature over 550 °C will yield rutile [5]. A mixture with a low pH value also leads to a greater yield of rutile [6,7]. The addition of certain elements, such as Cu and Ce, can influence particle growth and the crystalline phase ratio. This could be due to the induced charge balance leading to vacancies, or because of grain boundary pinning [8,9].

Amorphous phase is generally considered to be detrimental to photocatalytic activity, due to a high number of defects, which act as recombination centers [10,11]. There is a growing body of literature, however, that focuses on the benefits of amorphous phase [12–14]. On its own, amorphous phase exhibits poor photocatalytic activity, due to the short lifetime of charge carriers [15,16], caused by a high

* Corresponding author.
E-mail address: peter.nadrah@zag.si (P. Nadrah).
[1] Present address: Lek d.d., Verovškova ulica 57, 1526 Ljubljana, Slovenia.

https://doi.org/10.1016/j.ceramint.2024.07.092
Received 29 March 2024; Received in revised form 20 June 2024; Accepted 7 July 2024
Available online 8 July 2024

concentration of oxygen defects and Ti^{3+} species. The combination of amorphous phase with crystalline materials and the formation of heterojunctions can, however, produce highly active materials [17]. The beneficial effect of amorphous phase in the degradation of caffeine, for example, has been attributed to the faster adsorption of oxygen molecules on the surface and the increased lifetime of photogenerated holes [14]. Amorphous phase is also present in Evonik P25 TiO_2, a commercial photocatalyst material known for its high activity, which is used as a benchmark in many scientific publications [18]. Unfortunately, the majority of reports on photocatalytic TiO_2 do not contain data regarding the amorphous phase of materials, rather only data with respect to the crystalline phases. Given the potential of amorphous phase to contribute to the photocatalytic activity of crystalline materials, it is worthwhile exploring photocatalysts containing various amounts of amorphous phase as well as the formation of different TiO_2 phases.

The main analytical methods used to either confirm the presence of or quantify the amount of amorphous phase in a sample are X-ray powder diffraction (XRD) and transmission electron microscopy (TEM), with each method presenting its own set of difficulties. In the former, an (external or internal) standard is needed and the diffraction patterns are solved for both the standard and the samples. Additionally, solving diffraction patterns to quantify both the phase content and amorphous phase is difficult, and often made for a specific crystallite size and strain [19,20]. TEM, on the other hand, can clearly show the difference between the crystalline parts, with the crystal lattice planes visible against the less ordered amorphous phase. The downside of this method is that it is difficult to quantify and it does not usually account for the whole sample. This may be resolved through the analysis of multiple locations on a sample divided by a grid, but this is a very time-consuming process.

The environment during the crystallization step can significantly influence crystal nucleation and growth, and thus determines the phase ratio in polymorphic materials. By adapting the environment during crystallization, we can therefore engineer the photocatalyst's structure. One parameter of synthesis that has been studied to a lesser extent is the addition of organic compounds during the synthesis process. Ouzzine et al. [21] investigated the addition of acetic acid and isopropanol as hydrolyzing agents during synthesis and reported their influence on the crystal composition of the final material. With the addition of acetic acid, thermal treatment yielded only anatase up to 500 °C, anatase and rutile between 500 °C and 800 °C, and only rutile above 800 °C. The addition of isopropanol yielded only the anatase phase up to 400 °C, mixed phases at 500 °C and only rutile at temperatures of 600 °C and above. The addition of isopropanol therefore decreased the temperature needed for the formation of rutile, as only rutile was present at temperatures of 600 °C and above. Wang et al. [22] compared the degradation of isopropanol in TiO_2 with different anatase:rutile ratios. Faster degradation was observed in the TiO_2 with higher ratios of anatase. They hypothesized that the amount of water adsorbed on the TiO_2 and the lower specific surface area may be responsible for the higher activity observed in the anatase phase compared to in the rutile phase. One recent research study [23] investigated the effect of the anatase, rutile and brookite ratios on the photocatalytic activity of hydrothermally synthesized TiO_2. An anatase:brookite ratio of 61:39 elicited the highest photodegradation rate of levofloxacin. They attributed the highest activity rate to the large specific surface area, the lowest charge recombination rate and the most negative flat potential. TiO_2 with an anatase: brookite ratio of 68:32 had a lower specific surface area and exhibited significantly lower activity. Shie and Weng [24] added ethanol during TiO_2 synthesis to achieve an anatase:rutile ratio of 59:41 - this ratio elicited the fastest photodegradation of formaldehyde, being the only sample out of five to surpass the activity of P25. The high activity was attributed to the "antenna effect" of rutile and the activation effect of the anatase phase. The influence of organic compounds during the hydrothermal synthesis of TiO_2 has not yet been thoroughly investigated, let alone specific parameters (with respect to the combination of organic compounds and the duration of hydrothermal treatment) determined to produce TiO_2 with the crystalline and amorphous phase ratios desired.

To determine the effect of this and the optimal conditions for the hydrothermal synthesis of TiO_2 with specific phase ratios, we investigated the effect of the addition of small amounts of selected organic compounds, namely isopropyl alcohol (IPA), acetone (ACE) and acetic acid (AA), during the hydrothermal crystallization of TiO_2. We studied the influence of these compounds on the development of crystalline phases and the amount of amorphous phase formed during 48 h of hydrothermal treatment, as well as the subsequent effect on the morphological and photocatalytic properties of the end material.

2. Materials and methods

2.1. Synthesis of TiO_2

Titanium oxysulphate ($TiOSO_4$) (Sigma Aldrich 29 % ≥ as TiO_2) was used as the titanium source. This precursor was dissolved in purified water at a ratio of 15 wt%, using magnetic stirring in ambient conditions. A 10 % ammonia solution, prepared by diluting a 25 % solution (Sigma-Aldrich, NH_4OH), was instantaneously added to the $TiOSO_4$ solution and the mixture stirred vigorously until a pH value of 8 was achieved. The moment the ammonia was added, a white viscous gel immediately started to form in the reaction mixture. The gel obtained was then filtered and rinsed several times to remove any sulphate and ammonium ions. The absence of sulphate ions in the filtrate was indicated by the absence of $BaSO_4$ upon mixing it with $BaCl_2$ (Kemika) - a salt that is insoluble in this particular medium. The rinsed gel was dispersed in purified water, using the amount required to attain a TiO_2 concentration of 5 wt%. Nitric acid (Sigma Aldrich, HNO_3 content ≥65 %) was added to the gel as a peptizing agent, utilizing a 1:1 M ratio between TiO_2 and HNO_3. The mixture was then dispersed, using a mechanical stirrer at 4500 rpm for at least 30 min. 30 g of the mixture was transferred into a standard Teflon-lined stainless-steel autoclave with a capacity of 50 mL, and the organic compounds -namely IPA, ACE and AA (all supplied by Honeywell) - were added to the autoclaves. The molar ratio between the TiO_2 and the organic compound was 1:0.5. The autoclaves were then sealed and put into a preheated oven at 200 °C. After 2 h, 4 h, 18 h and 48 h of treatment the autoclaves were taken out of the oven and left to cool at an ambient temperature. The samples obtained were then thoroughly rinsed with purified water and dried in an oven for 24 h at 40 °C.

2.2. Characterization

X-ray powder diffraction (XRD) was used to determine the ratios between anatase, rutile and brookite as well as the amount of amorphous phase in the samples. A θ/θ diffractometer (PANalytical Empyrean, The Netherlands) equipped with a real time multiple strip (RTMS) detector (PIXcel 1D, PANalytical, The Netherlands) with Cu Kα radiation was used for the analysis, with the voltage set at 45 kV and a current of 40 mA. The diffraction was measured between 20 and 80° 2θ with a 0.02° 2θ step size and a virtual time of 250 s per step. On the side of the incident beam we used a 0.25° divergence slit and 0.5° anti-scattering slit, 0.04 rad Soller slits and a 10 mm copper mask. The samples were prepared in a 16 mm radius holder, filling them from the back to avoid preferential orientation.

The crystallite size of the anatase and rutile phases were calculated from the integral broadening of the reflection peaks using the Scherrer equation (1), where τ is the mean crystallite size, λ the X-ray wavelength, β_m the integral breadth of the sample, β_s the standard integral breadth and θ the Bragg angle, using a shape factor value, K, of 0.89 and the LaB_6 standard to account for the instrumental broadening. The crystallite sizes were calculated from peaks at approx. 25.3° 2θ, belonging to the reflection of anatase (101), and the peak at approx. 27.4° 2θ, belonging to the reflection of rutile (110).

$$\tau = \frac{K\lambda}{\sqrt{\beta_m^2 - \beta_s^2}\cos\theta} \quad (1)$$

The Rietveld and reference intensity ratio methods were combined to determine the amorphous and crystalline fractions in the samples. To this end, 10 wt% α−Al_2O_3 (NIST 676a [25]) was mixed with the samples and treated as an additional phase in the refinements [19,26]. The refined weight fractions of the individual crystalline phases (W_{ic}) were thus rescaled with respect to the known weight fraction of the added standard (W_s). The aim of this was to determine the actual weight (W_i) of each crystalline phase, according to the equation

$$W_i = \frac{1}{1 - W_s}\left[\left(\frac{W_S}{W_{SC}}\right)W_{ic}\right] \quad (2)$$

where W_{sc} is the refined weight fraction of the internal standard. By knowing the weight fractions of each of the crystalline phases, the amorphous fraction (W_a) is therefore given by the difference between 1 and the "as-received" components (W_i), i.e. the TiO_2 polymorphs in the specimens, as follows:

$$W_a = 1 - \sum_i W_i \quad (3)$$

The errors associated with the calculation of both the amorphous and crystalline phase fractions were calculated according to the procedure proposed by Madsen and Scarlett [27]. The Rietveld data analysis was assessed using the GSAS-EXPGUI software suite [28,29]. Instrumental broadening, determined through the refinement of the LaB_6 standard (NIST SRM 660b), was considered in all Rietveld refinements. These were accomplished by refining the following parameters: scale-factors, zero-point, 6 coefficients of the shifted Chebyshev function to fit the background, and unit cell parameters. The profile was modelled using the Thompson-Cox-Hasting formulation of the pseudo-Voigt function [30]. Two Lorentzian (L_X and L_Y) terms, peak correction for asymmetry, as well as sample displacement effects were all refined. On the contrary, the Gaussian parameter (G_W, an angle independent term) of the pseudo-Voigt profile shape function of the phases constituting the samples was constrained to the value obtained for α-alumina (NIST SRM 676a). The starting atomic parameters for anatase, rutile, and brookite, respectively described in the space groups $I4_1/amd$, $P4_2/mnm$ and $Pbca$, were taken from the literature [5,31]. The BET specific surface area was determined using nitrogen adsorption-desorption isotherms at 77 K using a Micrometrics ASAP 2020 instrument (USA). Micrographs of the samples for determining size and morphology were taken on a probe Cs-corrected Scanning Transmission Electron Microscope (STEM), model JEOL ARM200 CF (Jeol Ltd., Tokyo, Japan). A small amount of the sample investigated was deposited on a lacey carbon coated Cu TEM grid in powder form and investigated at an accelerating voltage of 80 kV.

2.3. Photocatalytic activity measurement

The photocatalytic activity of the samples was measured in a sealed gas-solid reactor system with continuous flow. IPA was used as the substrate for catalysis. The concentrations of IPA and ACE (the first oxidation product of IPA degradation) were continually monitored using Fourier-transform infrared spectroscopy. A schematic diagram of the reactor system has been published previously [32]. Approximately 40 mg of the sample was evenly spread over a glass disc, 60 mm in diameter, and put into the reactor, which was then hermetically sealed. The air in the reactor was directed through a dryer to lower the relative humidity to below 6 %. IPA was then injected into the reactor and allowed to evaporate. When the adsorption-desorption equilibrium was reached (at approx. 1 h), the sample was illuminated with a Xenon lamp producing light in both UV (approx. 20 W/m^2 in 300–400 nm) and the visible region (approx. 240 W/m^2 in 400–800 nm). The degree of activity was calculated from the slope of a linear fit to the initial linear section (covering a 6 min time span) of the ACE concentration curve.

Photocatalytic reaction cycles were performed as detailed above, with one slight modification (~33 % relative humidity instead of <6 %), maintaining at least 16 h between each run. Each cycle consisted of a 30-min period of irradiation with UV and visible light.

2.4. Diffuse reflectance spectroscopy

Samples were prepared as a 1 w/w% mixture with $BaSO_4$ (Kemika). The spectra were collected in the range 250–800 nm using a 1 nm step and a 12 cm integrating sphere (PerkinElmer Lambda 1050) with the specular component excluded. The resulting reflectance was divided by the reflectance of pure $BaSO_4$.

3. Results and discussion

The hydrothermal synthesis of TiO_2 from titanium oxysulphate over 2, 4, 18 or 48 h, with and without the addition of various organic compounds (IPA, ACE, AA and without as a control) yielded 16 different TiO_2 samples. Each sample was named in the format T-*x*-*y*, where *x* and *y* represent the organic compounds added (IPA, ACE, AA, none) and the duration of hydrothermal treatment in hours (2, 4, 18, 48), respectively. XRD analysis was performed with Al_2O_3 as an internal standard so as to determine the absolute phase contents, including that of the amorphous phase. The content of the crystalline phases and the amorphous phase in the synthesized TiO_2 were calculated from diffractograms, with the results summarized in Fig. 1. The general trend observed is a decrease in the amount of amorphous phase as the duration of hydrothermal treatment increases, and an increase in the rutile content at the expense of anatase and brookite. This is to be expected, since rutile is the most thermodynamically stable crystalline phase and is generally the final product of the crystallization and crystal reforming process. The various different sample groups (i.e. T-none, T-IPA, T-ACE and T-AA) exhibit different rates of crystallization and phase transitions according to the duration of hydrothermal treatment. The time-dependent evolution of the various phase contents is presented in Fig. 2. T-none features one of the fastest crystallization rates of all the sample groups (Fig. 2A). Anatase increases initially but then decreases (Fig. 2B). Some, although not all, of this increase can be attributed to crystallization from the amorphous phase. The rutile content steadily increases (Fig. 2C), while the brookite content steadily decreases (Fig. 2D). In addition to the expected transition of anatase to rutile, a transition from brookite to anatase can also be observed, since the increase in anatase between 2 and 4 h is greater than the concurrent decrease in the amorphous phase content. While this is unusual, it has been observed previously, having been reported by Zhu et al. [33]. Their observation yielded the concept of a critical grain size of brookite D_c, which is the size at which brookite transforms to rutile. Particles smaller than D_c transform to anatase and

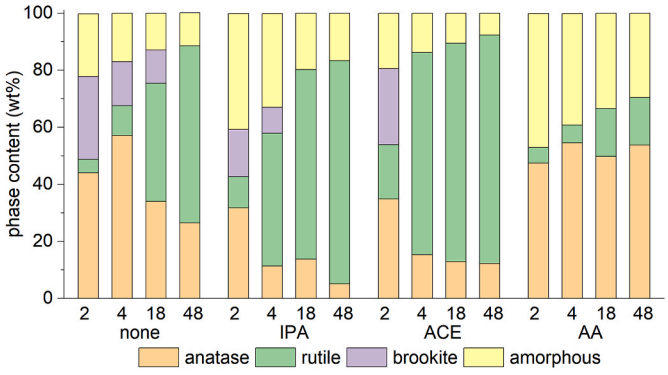

Fig. 1. Absolute content of the amorphous and crystalline phases, as determined by XRD. 2, 4, 18 and 48 on the x-axis refer to the hydrothermal treatment time in hours. None, IPA, ACE and AA refer to the organic compounds added.

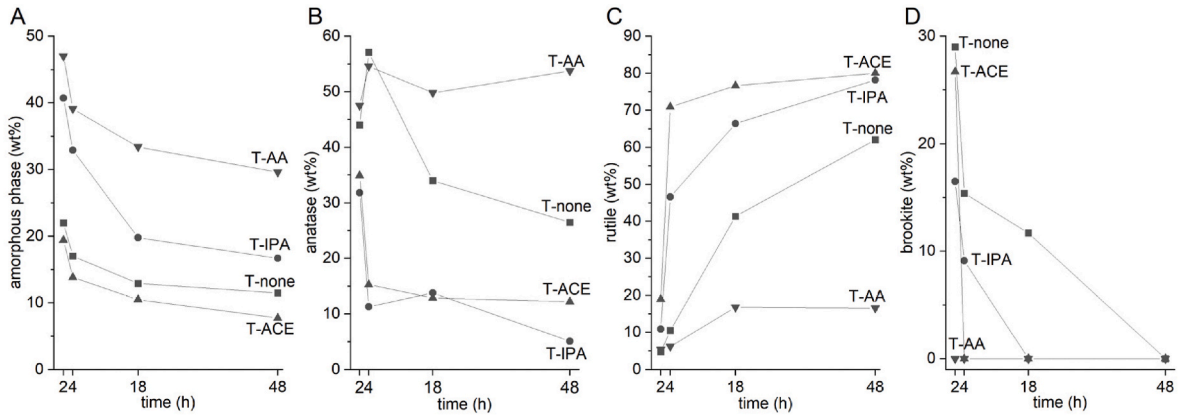

Fig. 2. Time evolution plots showing the content of (A) amorphous phase, (B) anatase, (C) rutile and (D) brookite for each sample group (T-none, T-IPA, T-ACE and T-AA) according to the duration of hydrothermal treatment. Note: scales on the y-axes differ.

then to rutile. After 2 h treatment, the T-IPA samples have a higher content of amorphous phase than T-none, and this continues to be higher even after 48 h (Fig. 2A). T-IPA exhibits the lowest content of anatase accompanied by the fastest decrease, with a small increase observed between 4 and 18 h (Fig. 2B). We cannot confirm whether the increase in the amount of anatase in the T-IPA samples is due to the transition of the amorphous phase or the transition of brookite to anatase. In T-IPA, a quick increase is observed in the rutile content alongside a gradual decrease in the brookite content (Fig. 2C and D). Between 4 and 18 h of hydrothermal treatment, brookite is either transformed into rutile or, partially, to anatase. T-ACE shows rapid crystallization and exhibits the lowest overall content of amorphous phase (Fig. 2A). This sample group has the lowest anatase content as well as the fastest decrease, with values comparable to the T-IPA group (Fig. 2B). The rutile content increases quickly and is higher than all the other samples at all four time points (Fig. 2C). In this group, brookite is transformed into anatase more quickly (between 2 and 4 h) compared to the more gradual transition observed in the groups T-none and T-IPA (Fig. 2D). T-AA exhibits the highest content of amorphous phase at any given time (Fig. 2A). The addition of acetic acid seems to inhibit crystallization, as these samples contain more amorphous phase than any other sample group. Interestingly, the anatase content stays at around 50 wt%, regardless of the duration of hydrothermal treatment (Fig. 2B). It is likely that the transition from anatase to rutile is taking place, but at a slow pace. At the same time, anatase can crystallize from the amorphous phase, such that content remains almost constant in the T-AA samples, regardless of the treatment duration. T-AA has the lowest rutile content, and this does not increase after 18 h (Fig. 2C). Brookite is absent from the T-AA samples. The above data show that ACE and IPA significantly favor the transition to rutile. AA, on the other hand, hinders the transition to both brookite and rutile. Additionally, AA decreases the rate of crystallization, given the slow decrease observed in the amorphous phase content. The less thermodynamically stable polymorphs, anatase and brookite, are usually produced via kinetically-controlled routes of synthesis [34], i.e. they may be formed from the amorphous phase more quickly, but will be transformed to rutile given the appropriate conditions. Rutile has lower bulk and a higher surface energy than anatase. Surface energy becomes the prevailing factor in smaller particles, so anatase is more stable than rutile when the particle size is small. Calculations have shown that, due to the bulk and surface energies, anatase is the most stable phase at a very small scale, when the particle size is below 11 nm, whereas brookite is most stable when the particle size is between 11 nm and 35 nm and rutile the most stable at particle sizes above 35 nm [35]. The energy differences are, however, sufficiently small that the reverse transitions are also possible when critical sizes apply [36].

Reflections in diffractograms can be indexed as anatase (JCPDS, no. 21–1272): 25.3°, 37.9°, 48.1°, 54.0°, 62.9°, 68.8°, 70.0°, 75.3°; as rutile (JCPDS, no. 21–1276): 27.4°, 36.1°, 39.2°, 41.2°, 44.0°, 54.3°, 56.5°, 62.8°, 64.0°, 69.0°, 69.8°; and as brookite (JCPDS, no. 04-022-2622): 25.3°, 30.5°, 47.9°, 54.1°, 62.9°. Broad peaks due to small crystallite size and low crystallinity in some samples cause overlap of certain reflections. Close-up images showing the time evolution of the diffractograms for anatase (101) (25.3°), rutile (110) (27.4°) and brookite (121) (30.5°) are presented in Fig. 3, while the full diffractograms are supplied in Figs. S1–S4. As the (120) and (111) reflections of brookite overlap with anatase (101), a less intensive reflection of brookite was selected [37]. In the case of T-none (Fig. 3A), a decrease in the peak width is observed in the anatase (101) reflection, which is associated with an increase in the crystallite size. The peak of the rutile (110) reflection increases substantially in all four sample groups. While the Rietveld analysis showed the presence of brookite, the peak of the (121) reflection exhibits a low intensity in T-none (Fig. 3A). T-IPA (Fig. 3B) exhibits a stark decrease in the intensity of anatase (101). This observation is similar to that for the T-ACE samples (Fig. 3C), but occurs to a lesser degree, with the anatase content in T-ACE-48 being higher than that of T-IPA-48. Across all the samples, the peak of brookite (121) is most evident in T-ACE-2. A narrowing of the peak of the anatase (101) reflection can be observed in T-AA (Fig. 3D).

The specific surface area (SSA) of the samples, presented in Fig. 4A, was determined by nitrogen sorption using the Brunauer-Emmet-Teller (BET) model. The average crystallite size of anatase and rutile, calculated using the Scherrer equation from the integral breadth of the anatase (101) and rutile (110) reflections at approx. 25.3° 2θ and 27.4° 2θ, respectively, are presented alongside the SSA data in Fig. 4A. The size of rutile in T-none-2 and T-AA-2 and the size of anatase in T-IPA-48 are not presented, as the respective content in these samples was too low to allow a reliable calculation. It should be noted that the Scherrer equation does not take into account the different shape of crystallites, as the same shape factor of 0.89 was used for all calculations to make it easier to compare the different phases. The average crystallite sizes calculated should therefore be viewed as values indicating the peak broadening rather than as absolute crystallite sizes. This holds especially true of rutile, which is present in the form of rods, with a high aspect ratio. Due to the overlap of anatase (101) and brookite (120)/(111), the crystallite size was also calculated using the peak of the anatase (200) reflection (at approx. 48.1° 2θ), which yielded comparable results (data not shown). The reaction conditions are not expected to produce porous materials, therefore the surface area can be related to the crystallite size. As depicted in Fig. 4, the SSA values are high when the length of the hydrothermal treatment is short. This is due to the small size of the crystallites, as shown by the calculations, and can be observed by the broad peaks evident in Fig. 3. In all cases, the SSA decreased as the duration of hydrothermal treatment was extended. The largest changes are seen at 2, 4 and 18 h. Prolonging the synthesis time to 48 h had less

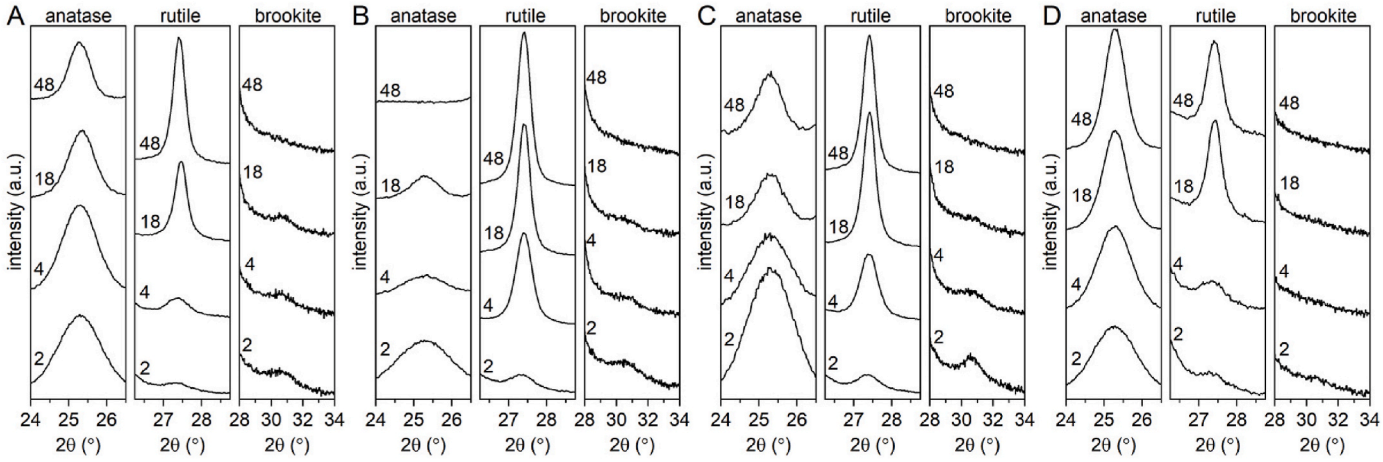

Fig. 3. Time evolution of the diffractograms in three regions (anatase (101), rutile (110) and brookite (121)) for the four different sample groups, T-none (A), T-IPA (B), T-ACE (C) and T-AA (D). The labels on the graphs refer to the duration of hydrothermal treatment (in hours). The plots are offset on the y-axis.

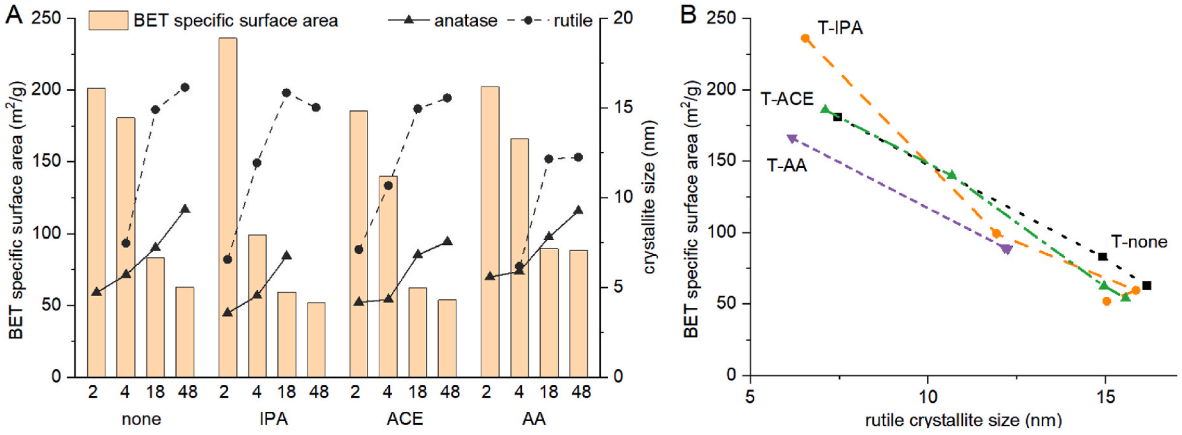

Fig. 4. A: BET specific surface area (bars) and crystallite size (symbols) of the anatase and rutile phases in the four different sample groups (T-none, T-IPA, T-ACE and T-AA). B: BET specific surface area versus the crystallite size of rutile.

of an effect on the SSA. In most cases, the decrease in SSA coincides with a decrease in the amorphous phase content, an increase in the rutile content and an increase in the crystallite size of both rutile and anatase. The size of anatase increases in all cases except in T-IPA-48, where the amount of anatase is too low for the reliable determination of size. The crystallite size of rutile, on the other hand, increases from 2 to 18 h, followed by a more modest increase or even a small decrease at 48 h. An increase in the crystallite size of rutile can be observed both in the case of a significant increase in rutile content (T-none), as well as in the case of only a slight increase (T-AA). A decrease in SSA is associated with the growth of rutile crystallites, as presented in Fig. 4B. In each sample group, the most significant decrease in SSA (from 4 to 18 h in T-none, from 2 to 4 h in T-IPA, from 4 to 18 h in T-ACE and from 4 to 18 h in T-AA) is associated with a large increase in the crystallite size of rutile, even if the rutile content does not substantially increase, as was the case with T-AA. An interesting observation is made when evaluating the difference in the SSA of the T-IPA and T-ACE samples between 2 and 4 h of hydrothermal treatment. A significant drop (from ~240 m^2/g to ~100 m^2/g) is observed in the SSA of the T-IPA samples, which coincides with significant growth in the rutile content (from 11 wt% to 47 wt%). The SSA of the T-ACE samples, however, only decreases from ~200 m^2/g to ~150 m^2/g over the same period, while the rutile content increases from 19 wt% to 71 wt%. As explained above, particle growth in TiO_2 is also associated with phase transition. Generally, the particles of anatase are smaller than those of rutile, which is mostly present in the form of larger, elongated particles [7,38].

To analyze the morphology and visually confirm the size of the crystallites, TEM analysis was performed on two samples (T-none-2 and T-none-4). The well-defined crystal planes of the T-none-2 sample can be seen in Fig. 5 (further micrographs at lower magnifications are presented in Fig. S5). The particles in the micrographs show typical planes throughout the individual particles, with barely any amorphous material visible at the edges of the crystals. The particles measure approximately 3–15 nm in diameter, which aligns well with the calculated values (Fig. 4A). The majority of the particles are loosely spherical in shape, with the presence of some truncated octahedrons (Fig. 5A), which is a typical shape for anatase. The other two polymorphs of TiO_2 could not be seen in the micrographs. The presence of rutile and brookite in T-none-2 is, however, confirmed by both XRD and selected area diffraction (SAED) patterns (Fig. 1 and Fig. S6). It is expected for particles to be prevalent in the anatase form, since this is the most stable polymorph of TiO_2 for particles of this size. In the case of T-none-2, however, the hydrothermal treatment was not long enough for particles to grow and transform into the rutile polymorph. The process of growth and transition has begun, but the reaction was stopped after 2 h of hydrothermal treatment. The micrographs of T-none-4 in Fig. 6 show well-defined crystals, similar to those seen in T-none-2. Rutile can be clearly seen in the form of elongated particles, with a pyramid-shaped end (further micrographs at lower magnifications are presented in Fig. S7). The rutile crystals are larger than those of anatase, measuring over 40 nm in length

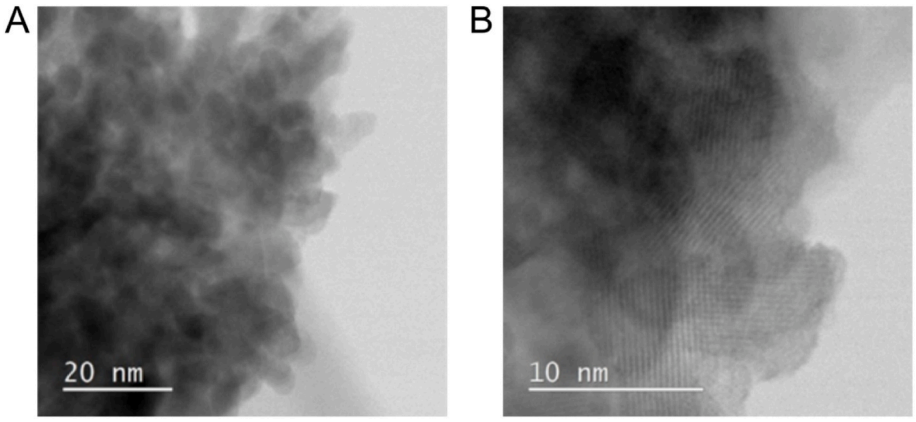

Fig. 5. TEM micrographs of the sample T-none-2 at two levels of magnification. The majority of the material is anatase, consisting of particles with diameters of 3–15 nm and possessing well-defined crystal planes.

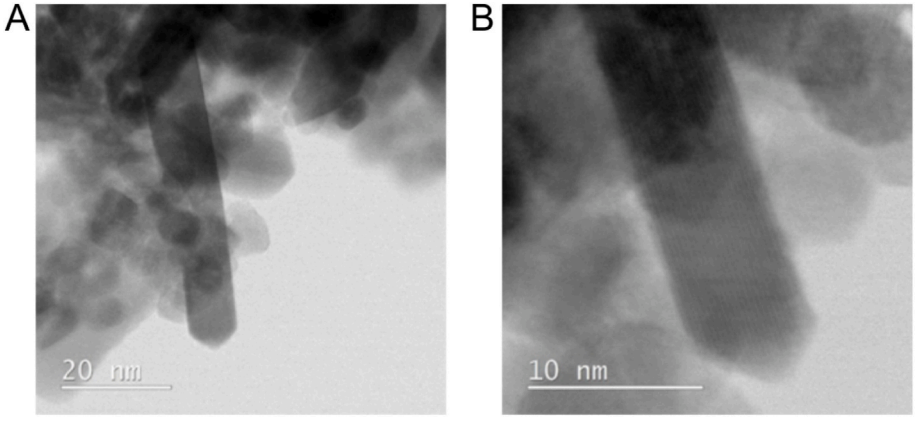

Fig. 6. TEM micrographs of the sample T-none-4 at two levels of magnification. The majority of particles are in the anatase polymorph, with some clearly-defined rutile particles present.

and approximately 10 nm in width. Even the anatase particles are larger in sample T-none-4 than in sample T-none-2, measuring about 7–20 nm as opposed to 3–15 nm. This is expected, due to the longer duration of the hydrothermal treatment. In the case of T-none-4, there is more time available for the crystallites to rearrange, transform into a thermodynamically more stable form and grow. XRD showed the brookite polymorph to be present in a significant amount (15 wt%), although this value was slightly lower when evaluated by SAED (Fig. S8)."It is apparent that longer hydrothermal treatment leads to particle growth and transition of the crystal form.

The photocatalytic activity of the synthesized samples was determined in a gas-solid system by monitoring the oxidation of isopropanol into acetone over a solid TiO_2 film irradiated with UV and visible light. Among the most prominent factors that influence photocatalytic activity are crystallinity and crystal phase composition, particle size, particle shape, SSA, optical absorption and surface chemistry [4,39]. The general trend in all samples is an increase in activity between 2 h of hydrothermal treatment and 4 h of treatment, which is followed by a decrease in activity in the 18 h and 48 h samples (Fig. 7). The fact that the samples that underwent 4 h of hydrothermal treatment exhibited the highest activity can be explained by the favourable combination of the increase in the crystalline phase content, whilst retaining a relatively high SSA compared to the 2-h samples. The lower activity of the 18- and 48-h samples compared to the 4-h samples is consistent with an increase in the rutile fraction (except for in the case of T-AA) and a decrease in the SSA. The small phase transitions evident in the T-AA samples can hardly be the major reason for the diminished activity, so it can therefore be

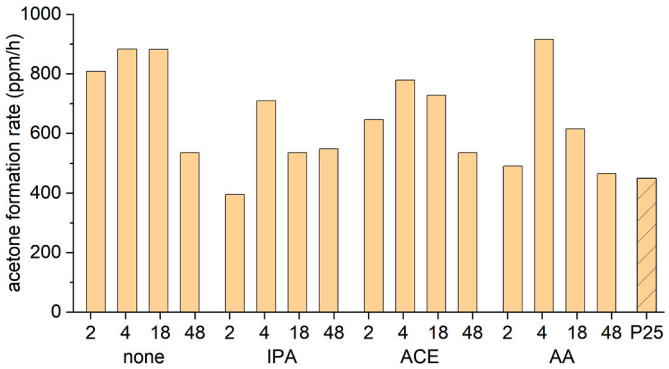

Fig. 7. Photocatalytic activity, presented as the formation rate of acetone produced from isopropanol, in all sample groups (T-none, T-IPA, T-ACE and T-AA), with P25 as a reference.

ascribed to a decrease in SSA and the concurrent particle growth, as would be expected. The samples without any organic compound added (T-none) are generally the most active. The activity in T-none-4 and T-none-18 is almost identical, despite their properties, such as SSA and phase composition, being fundamentally different. The longest hydrothermal treatment, i.e. 48 h, yielded the least active materials in three out of the four sample groups. The exception is T-IPA, where the activity of T-IPA-48 is on a par with that of T-IPA-18. A shift in phase composition seems to play an important role in increasing the activity – to the

extent that it offsets the decrease in SSA. With the exception of T-IPA-2, all materials display higher activity than the reference, P25. The differences in activity cannot be easily connected with any individual property. Rather, we hypothesize that a favourable combination of crystallinity, phase composition and SSA contributes to the increase in activity.

Five cycles of the photocatalytic reaction were performed for the two photocatalysts with the highest activity, namely T-none-18 and T-AA-4. The experiment was conducted in the reaction chamber at a relative humidity of approx. 33 %, so the absolute values are not directly comparable with the activity values shown in Fig. 7. The results for T-none-18 (Fig. S9) show a slight increase in activity after the first cycle, followed by steady activity between 125 % and 131 % of the initial value from thereon in. We cannot say whether this is due to an experimental error in the first cycle or due to activation of the photocatalyst with UV light. T-AA-4 exhibits steady activity between 95 % and 102 % of the initial value. These results indicate good stability in these two photocatalysts.

Little variation is seen between the diffuse reflectance measurements of the selected samples (Fig. S10). The calculated band gaps were 3.01 eV and 3.05 eV for T-none-4 and T-none-18, respectively, and 3.09 eV and 2.99 eV for T-AA-4 and T-AA-18, respectively. Most values lie between the respective values for rutile (3.0 eV) and anatase (3.2 eV). To analyze the effect of photocatalysis on the absorption and reflectance of light, T-none-18 and T-AA-4 were analysed after 5 cycles of photocatalytic measurements (2.5 h of UV and visible light irradiation). The values obtained (3.03 eV and 3.10 eV for T-none-18 and T-AA-4, respectively) match well against the values of the pristine samples obtained before the irradiation.

4. Conclusions

A total of 16 TiO_2 samples were synthesized by varying two parameters - namely, the organic compound added (IPA, ACE, AA or none) and the duration of the hydrothermal treatment. All samples exhibited a decrease in the amount of amorphous phase and an increase in the amount of rutile as the duration of the hydrothermal treatment increased. The organic compounds added significantly affected the ratios of the crystalline and amorphous phase. The T-none samples exhibited a gradual increase in the amount of rutile as the duration of the hydrothermal treatment increased. The T-ACE samples exhibited the least amount of amorphous phase and the fastest transition into rutile. The T-IPA samples exhibited accelerated rutile growth compared to T-none, but not to the same extent as in T-ACE. The T-AA samples contain the highest amount of amorphous phase, with anatase being the primary crystalline phase. Furthermore, a decrease in the specific surface area of the materials was observed when the duration of hydrothermal treatment was longer, which aligns well with rutile crystallite growth. While anatase crystallites grow steadily up to 48 h, rutile particles only grow up to 18 h, with a subsequent inhibition of growth or a slight decrease in size. Particle growth also determines the phase transitions, based on the stability of the polymorphs at a specific size. Photocatalytic activity, measured as the formation rate of acetone from isopropanol, was highest in all sample groups after 4 h of hydrothermal treatment, with shorter (2 h) and longer (18 and 48 h) periods of treatment leading to the production of less active materials. Five cycles of photocatalytic tests showed good stability with respect to the activity of the two selected samples (T-none-18 and T-AA-4). The results presented demonstrate that organic additives affect phase transition rates and significantly influence the phase composition of hydrothermally synthesized TiO_2, even when the duration of hydrothermal treatment is short (2 or 4 h). The addition of organic compounds presents a route to tailor the phase composition of TiO_2, by either increasing (IPA or ACE) or decreasing (AA) the speed of crystallization and conversion to rutile. By combining these with a specific duration of hydrothermal treatment, several desirable materials can be obtained. The combination of AA with a very short treatment duration (2 h) yields TiO_2 with equal amounts of anatase and amorphous phase and little rutile. The fastest way to get highly crystalline TiO_2 with a high rutile content (71 %) is to use ACE and a short treatment time (4 h), as longer treatment times further increase the rutile content up to only 80 %. A TiO_2 combining all four of the phases considered can be synthesized using either IPA or ACE and a very short treatment duration (2 h), or without the addition of any compound, using very short to moderate treatment times (2–18 h). The optimal combination should be selected based on the final ratio desired between the four different phases.

CRediT authorship contribution statement

Nejc Rozman: Writing – review & editing, Writing – original draft, Visualization, Validation, Methodology, Investigation, Conceptualization. **Andrijana Sever Škapin:** Writing – review & editing, Writing – original draft, Supervision, Resources, Project administration, Funding acquisition, Conceptualization. **David M. Tobaldi:** Writing – review & editing, Validation, Methodology, Formal analysis. **Goran Dražić:** Writing – review & editing, Validation, Investigation, Formal analysis. **Peter Nadrah:** Writing – review & editing, Writing – original draft, Visualization, Supervision, Methodology, Investigation, Conceptualization.

Declaration of competing interest

The authors declare that they have no known competing financial interests or personal relationships that could have appeared to influence the work reported in this paper.

Acknowledgements

We acknowledge the financial support by the Slovenian Research and Innovation Agency (Grants no. NC-0017, J2-4441 and P2-0273).

Appendix A. Supplementary data

Supplementary data to this article can be found online at https://doi.org/10.1016/j.ceramint.2024.07.092.

References

[1] L. Liu, X. Chen, Titanium dioxide nanomaterials: self-structural modifications, Chem. Rev. 114 (2014) 9890–9918, https://doi.org/10.1021/cr400624r.
[2] H.G. Yang, C.H. Sun, S.Z. Qiao, J. Zou, G. Liu, S.C. Smith, H.M. Cheng, G.Q. Lu, Anatase TiO2 single crystals with a large percentage of reactive facets, Nature 453 (2008) 638–641, https://doi.org/10.1038/nature06964.
[3] D.M. Tobaldi, L. Lajaunie, N. Rozman, A.P.F. Caetano, M.P. Seabra, A. Sever Škapin, R. Arenal, J.A. Labrincha, Impact of the absolute rutile fraction on TiO2 visible-light absorption and visible-light-promoted photocatalytic activity, J. Photochem. Photobiol., A A 382 (2019) 111940, https://doi.org/10.1016/j.jphotochem.2019.111940.
[4] J. Schneider, M. Matsuoka, M. Takeuchi, J. Zhang, Y. Horiuchi, M. Anpo, D. W. Bahnemann, Understanding TiO2 photocatalysis: mechanisms and materials, Chem. Rev. 114 (2014) 9919–9986, https://doi.org/10.1021/cr5001892.
[5] E. Meagher, G.A. Lager, Polyhedral thermal expansion in the TiO 2 polymorphs; refinement of the crystal structures of rutile and brookite at high temperature, Can. Mineral. 17 (1979) 77–85.
[6] G.-Y. Zhang, Y.-Q. Sun, D.-Z. Gao, Y.-Y. Xu, Quasi-cube ZnFe2O4 nanocrystals: hydrothermal synthesis and photocatalytic activity with TiO2 (Degussa P25) as nanocomposite, Mater. Res. Bull. 45 (2010) 755–760, https://doi.org/10.1016/j.materresbull.2010.03.025.
[7] N. Rozman, L. Škrlep, M. Gaberšček, A. Sever-Škapin, Tuning the photocatalytic activity of nanocrystalline titania by phase composition control and nitrogen doping, using different sources of nitrogen, Acta Chim. Slov. 61 (2014) 506–516.
[8] R.D. Shannon, J.A. Pask, Kinetics of the anatase-rutile transformation, J. Am. Chem. Soc. 48 (1965) 391–398, https://doi.org/10.1111/j.1151-2916.1965.tb14774.x.
[9] D.M. Tobaldi, N. Rozman, M. Leoni, M.P. Seabra, A.S. Škapin, R.C. Pullar, J. A. Labrincha, Cu–TiO $_2$ hybrid nanoparticles exhibiting tunable photochromic behavior, J. Phys. Chem. C 119 (2015) 23658–23668, https://doi.org/10.1021/acs.jpcc.5b07160.

[10] B. Ohtani, Y. Ogawa, S. Nishimoto, Photocatalytic activity of Amorphous−Anatase mixture of titanium(IV) oxide particles suspended in aqueous solutions, J. Phys. Chem. B 101 (1997) 3746–3752, https://doi.org/10.1021/jp962702+.
[11] M.J. Torralvo, J. Sanz, I. Sobrados, J. Soria, C. Garlisi, G. Palmisano, S. Çetinkaya, S. Yurdakal, V. Augugliaro, Anatase photocatalyst with supported low crystalline TiO2: the influence of amorphous phase on the activity, Appl. Catal., B 221 (2018) 140–151, https://doi.org/10.1016/j.apcatb.2017.08.089.
[12] C. Randorn, J.T.S. Irvine, P. Robertson, Synthesis of visible-light-activated yellow amorphous photocatalyst, Int. J. Photoenergy 2008 (2008) e426872, https://doi.org/10.1155/2008/426872.
[13] S. Zeng, L. Zhang, W. Wang, D. Shao, H. Hao, Hydrogen evolution based on the electrons/protons stored on amorphous TiO2, Phys. Chem. Chem. Phys. 19 (2017) 29053–29056, https://doi.org/10.1039/C7CP06067J.
[14] M. Krivec, R.A. Segundo, J.L. Faria, A.M.T. Silva, G. Dražić, Low-temperature synthesis and characterization of rutile nanoparticles with amorphous surface layer for photocatalytic degradation of caffeine, Appl. Catal., B 140–141 (2013) 9–15, https://doi.org/10.1016/j.apcatb.2013.03.045.
[15] S. Pan, X. Liu, M. Guo, S. fung Yu, H. Huang, H. Fan, G. Li, Engineering the intermediate band states in amorphous Ti3+-doped TiO2 for hybrid dye-sensitized solar cell applications, J. Mater. Chem. A 3 (2015) 11437–11443, https://doi.org/10.1039/C5TA00956A.
[16] Y. Ide, N. Inami, H. Hattori, K. Saito, M. Sohmiya, N. Tsunoji, K. Komaguchi, T. Sano, Y. Bando, D. Golberg, Y. Sugahara, Remarkable charge separation and photocatalytic efficiency enhancement through interconnection of TiO2 nanoparticles by hydrothermal treatment, Angew. Chem. Int. Ed. 55 (2016) 3600–3605, https://doi.org/10.1002/anie.201510000.
[17] S. Sun, P. Song, J. Cui, S. Liang, Amorphous TiO2 nanostructures: synthesis, fundamental properties and photocatalytic applications, Catal. Sci. Technol. 9 (2019) 4198–4215, https://doi.org/10.1039/C9CY01020C.
[18] D.M. Tobaldi, R.C. Pullar, M.P. Seabra, J.A. Labrincha, Fully quantitative X-ray characterisation of Evonik aeroxide TiO2 P25®, Mater. Lett. 122 (2014) 345–347, https://doi.org/10.1016/j.matlet.2014.02.055.
[19] A.F. Gualtieri, Accuracy of XRPD QPA using the combined Rietveld–RIR method, J. Appl. Crystallogr. 33 (2000) 267–278, https://doi.org/10.1107/S002188989901643X.
[20] L.B. McCusker, R.B. Von Dreele, D.E. Cox, D. Louër, P. Scardi, Rietveld refinement guidelines, J. Appl. Crystallogr. 32 (1999) 36–50, https://doi.org/10.1107/S0021889898009856.
[21] M. Ouzzine, M.A. Lillo-Ródenas, A. Linares-Solano, Photocatalytic oxidation of propene in gas phase at low concentration by optimized TiO2 nanoparticles, Appl. Catal., B 134–135 (2013) 333–343, https://doi.org/10.1016/j.apcatb.2013.01.035.
[22] Y. Wang, H. Wang, X. Tan, Study of 2-propanol photocatalytic degradation on surface of phase-ratio-controlled TiO2 nanoparticles, Trans. Tianjin Univ. 24 (2018) 1–7, https://doi.org/10.1007/s12209-017-0077-7.
[23] X. Lin, M. Sun, B. Gao, W. Ding, Z. Zhang, S. Anandan, A. Umar, Hydrothermally regulating phase composition of TiO2 nanocrystals toward high photocatalytic activity, J. Alloys Compd. 850 (2021) 156653, https://doi.org/10.1016/j.jallcom.2020.156653.
[24] L. Shi, D. Weng, Highly active mixed-phase TiO2 photocatalysts fabricated at low temperatureand the correlation between phase compositionand photocatalytic activity, J. Environ. Sci. 20 (2008) 1263–1267, https://doi.org/10.1016/S1001-0742(08)62219-6.
[25] J.P. Cline, R.B. Von Dreele, R. Winburn, P.W. Stephens, J.J. Filliben, Addressing the amorphous content issue in quantitative phase analysis: the certification of NIST standard reference material 676a, Acta Crystallogr A Found Crystallogr 67 (2011) 357–367, https://doi.org/10.1107/S0108767311014565.
[26] A.F. Gualtieri, G. Brignoli, Rapid and accurate quantitative phase analysis using a fast detector, J. Appl. Crystallogr. 37 (2004) 8–13, https://doi.org/10.1107/S0021889803022052.
[27] I.C. Madsen, N.V.Y. Scarlett, Chapter 11. Quantitative phase analysis, in: R. E. Dinnebier, S.J.L. Billinge (Eds.), Powder Diffraction, Royal Society of Chemistry, Cambridge, 2008, pp. 298–331, https://doi.org/10.1039/9781847558237-00298.
[28] B.H. Toby, *EXPGUI* , a graphical user interface for *GSAS*, J. Appl. Crystallogr. 34 (2001) 210–213, https://doi.org/10.1107/S0021889801002242.
[29] R. Von Dreele, A. Larson, General structure analysis system (GSAS), Los Alamos Natl, Lab. Rep. LAUR 748 (2004) 86–748.
[30] P. Thompson, D.E. Cox, J.B. Hastings, Rietveld refinement of Debye–Scherrer synchrotron X-ray data from Al $_2$ O $_3$, J. Appl. Crystallogr. 20 (1987) 79–83, https://doi.org/10.1107/S0021889887087090.
[31] C.J. Howard, T.M. Sabine, F. Dickson, Structural and thermal parameters for rutile and anatase, Acta Crystallogr. B Struct. Sci. 47 (1991) 462–468, https://doi.org/10.1107/S010876819100335X.
[32] N. Rozman, D. Tobaldi, U. Cvelbar, H. Puliyalil, J. Labrincha, A. Legat, A. Sever Škapin, Hydrothermal synthesis of rare-earth modified titania: influence on phase composition, optical properties, and photocatalytic activity, Materials 12 (2019) 713, https://doi.org/10.3390/ma12050713.
[33] K.-R. Zhu, M.-S. Zhang, J.-M. Hong, Z. Yin, Size effect on phase transition sequence of TiO2 nanocrystal, Mater. Sci. Eng., A 403 (2005) 87–93, https://doi.org/10.1016/j.msea.2005.04.029.
[34] G. Símonarson, S. Sommer, A. Lotsari, B. Elgh, B.B. Iversen, A.E.C. Palmqvist, Evolution of the polymorph selectivity of titania formation under acidic and low-temperature conditions, ACS Omega 4 (2019) 5750–5757, https://doi.org/10.1021/acsomega.8b03440.
[35] H. Zhang, J.F. Banfield, Understanding polymorphic phase transformation behavior during growth of nanocrystalline aggregates: insights from TiO $_2$, J. Phys. Chem. B 104 (2000) 3481–3487, https://doi.org/10.1021/jp000499j.
[36] A. Di Paola, M. Bellardita, L. Palmisano, Brookite, the least known TiO2 photocatalyst, Catalysts 3 (2013) 36–73, https://doi.org/10.3390/catal3010036.
[37] D. Reyes-Coronado, G. Rodríguez-Gattorno, M.E. Espinosa-Pesqueira, C. Cab, R. de Coss, G. Oskam, Phase-pure TiO2 nanoparticles: anatase, brookite and rutile, Nanotechnology 19 (2008) 145605, https://doi.org/10.1088/0957-4484/19/14/145605.
[38] J. Yu, A.L. Godiksen, A. Mamahkel, F. Søndergaard-Pedersen, T. Rios-Carvajal, M. Marks, N. Lock, S.B. Rasmussen, B.B. Iversen, Selective catalytic reduction of NO using phase-pure anatase, rutile, and brookite TiO $_2$ nanocrystals, Inorg. Chem. 59 (2020) 15324–15334, https://doi.org/10.1021/acs.inorgchem.0c02304.
[39] M.A. Henderson, A surface science perspective on TiO2 photocatalysis, Surf. Sci. Rep. 66 (2011) 185–297, https://doi.org/10.1016/j.surfrep.2011.01.001.